CD44: a novel synaptic cell adhesion molecule regulating structural and functional plasticity of dendritic spines

Matylda Roszkowska[a,b], Anna Skupien[a], Tomasz Wójtowicz[c], Anna Konopka[a], Adam Gorlewicz[a], Magdalena Kisiel[c], Marek Bekisz[d], Blazej Ruszczycki[e], Hubert Dolezyczek[a], Emilia Rejmak[f], Ewelina Knapska[g], Jerzy W. Mozrzymas[c], Jakub Wlodarczyk[b], Grzegorz M. Wilczynski[a], and Joanna Dzwonek[a,*]

[a]Laboratory of Molecular and Systemic Neuromorphology, [b]Laboratory of Cell Biophysics, [d]Laboratory of Visual System, [e]Laboratory of Imaging Tissue Structure and Function, [f]Laboratory of Neurobiology, and [g]Laboratory of Emotions Neurobiology, Nencki Institute of Experimental Biology, Polish Academy of Sciences, 02-093 Warsaw, Poland; [c]Laboratory of Neuroscience, Department of Biophysics, Wroclaw Medical University, 50-368 Wroclaw, Poland

ABSTRACT **Synaptic cell adhesion molecules regulate signal transduction, synaptic function, and plasticity. However, their role in neuronal interactions with the extracellular matrix (ECM) is not well understood. Here we report that the CD44, a transmembrane receptor for hyaluronan, modulates synaptic plasticity. High-resolution ultrastructural analysis showed that CD44 was localized at mature synapses in the adult brain. The reduced expression of CD44 affected the synaptic excitatory transmission of primary hippocampal neurons, simultaneously modifying dendritic spine shape. The frequency of miniature excitatory postsynaptic currents decreased, accompanied by dendritic spine elongation and thinning. These structural and functional alterations went along with a decrease in the number of presynaptic Bassoon puncta, together with a reduction of PSD-95 levels at dendritic spines, suggesting a reduced number of functional synapses. Lack of CD44 also abrogated spine head enlargement upon neuronal stimulation. Moreover, our results indicate that CD44 contributes to proper dendritic spine shape and function by modulating the activity of actin cytoskeleton regulators, that is, Rho GTPases (RhoA, Rac1, and Cdc42). Thus CD44 appears to be a novel molecular player regulating functional and structural plasticity of dendritic spines.**

Monitoring Editor
Mark H. Ginsberg
University of California, San Diego

Received: Jun 15, 2016
Revised: Sep 19, 2016
Accepted: Oct 12, 2016

INTRODUCTION

Interactions between the extracellular matrix in the brain and neuronal cells play an important role in regulating signal transduction, synaptic function, and plasticity (Dityatev and Schachner, 2003). The remodeling of extracellular matrix (ECM) components has a profound effect on overall synaptic machinery (Dityatev and Rusakov, 2011; Wlodarczyk *et al.*, 2011; Thalhammer and Cingolani, 2014) and affects synaptic receptor composition and mobility (Groc *et al.*, 2007; Frischknecht *et al.*, 2009) and dendritic spine shape (Bilousova *et al.*, 2006; Wang *et al.*, 2008; Michaluk *et al.*, 2011). However, knowledge of the molecular mechanisms involved in signal transmission from the extracellular environment to neuronal cells is far from complete. Synaptically expressed cell adhesion molecules (CAMs) are specialized proteins that contribute to the proper establishment of synaptic contacts by ensuring proper organization of their structure and influencing synaptic plasticity (Missler *et al.*, 2012). The significance of synaptic CAMs in processes of synapse formation and signal transmission between neurons is only beginning to be known. The discovery of novel synaptic CAMs, together with knowledge of the ways in which CAMs function at highly specific connecting hubs in the nervous system, is an important step toward understanding information transfer in the brain (Missler *et al.*, 2012; Conant *et al.*, 2015).

This article was published online ahead of print in MBoC in Press (http://www.molbiolcell.org/cgi/doi/10.1091/mbc.E16-06-0423) on October 19, 2016.

The authors declare no competing financial interests.

*Address correspondence to: Joanna Dzwonek (j.dzwonek@nencki.gov.pl).

Abbreviations used: CAMs, cell adhesion molecules; cLTP, chemical long-term potentiation; ECM, extracellular matrix; FISH, fluorescence in situ hybridization; FRET, Förster resonance energy transfer; HA, hyaluronic acid; mEPSC, miniature excitatory postsynaptic current; PSD-95, postsynaptic density protein 95.

Supplemental Material can be found at:
http://www.molbiolcell.org/content/suppl/2016/10/17/mbc.E16-06-0423v1.DC1.html

The major component of the ECM in the brain is hyaluronic acid (HA), which was shown to contribute to many plastic processes in the nervous system (for review, see Wlodarczyk *et al.*, 2011). Hyaluronic acid can influence cell behavior by interacting with cell surface receptors, including the CD44 adhesion molecule. To date, CD44 has not been identified as a synaptic CAM. We recently showed that it plays a pivotal role in regulating the morphogenesis of dendritic trees (Skupien *et al.*, 2014). Furthermore, the silencing of CD44 expression during the early development of neuronal cells exerted a protective effect on young neurons that were exposed to a toxic concentration of glutamate (Skupien *et al.*, 2014).

In this study, we apply state-of-the-art molecular biology techniques to elucidate the role of CD44 protein in dendritic spine remodeling and synaptic plasticity. A combination of electron microscopy, immunogold labeling, in situ hybridization, Förster resonance energy transfer (FRET)–based methods, and electrophysiological recordings unravel yet-uncharacterized contributions of CD44 adhesion molecule to proper functioning of mature hippocampal neurons.

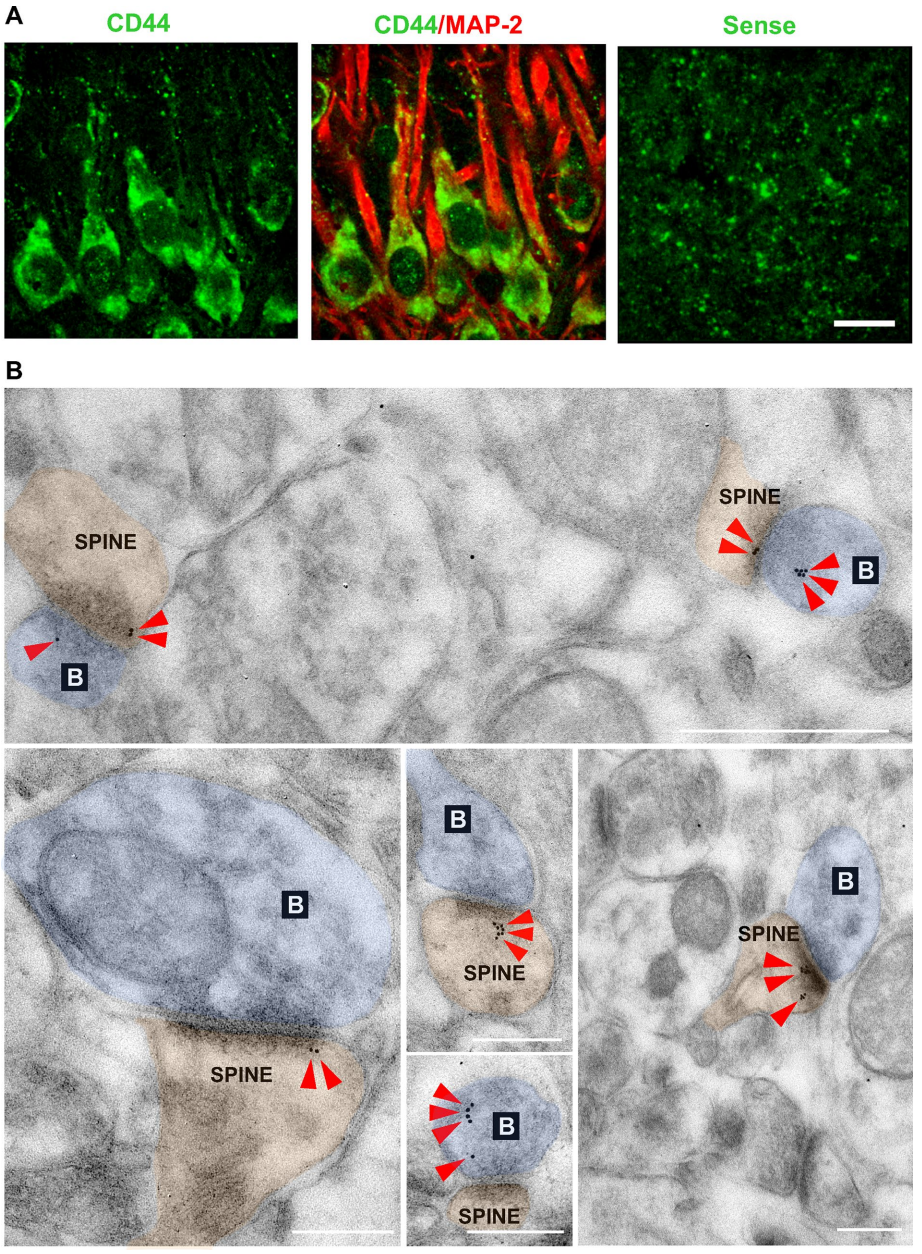

FIGURE 1: CD44 is expressed by neurons in adult rat brain and localizes at synapses. (A) In situ hybridization signal (CD44 mRNA, antisense probe, green) colocalizes with immunofluorescence of anti–MAP-2 (red) antibody in the CA3 field of the rat hippocampus. Hybridization with the sense probe is shown as a control. Scale bar, 15 μm. (B) Immunogold electron microscope detection (after embedding) of CD44 in the CA3 region of the hippocampus. Immunogold particles indicating CD44IR (red arrowheads) are present within the dendritic spines (SPINE, orange) and axonal boutons (B, blue). Scale bar, 250 nm. Distribution of CD44 in dendritic spines and presynaptic boutons was quantified. For $\chi^2 = 1140$ or 217, respectively, and one degree of freedom, $p < 000001$, and so the distribution pattern of gold-labeled CD44 in both compartments is significantly different from random, in contrast to the labeling with nonimmune IgG control antibody.

RESULTS

CD44 localizes at hippocampal synapses

We previously investigated CD44 expression patterns in the developing rat brain (Skupien *et al.*, 2014). We found that protein abundance decreases in the mature neuronal tissue, but it can still be detected in the brain of adult animals. To characterize CD44 expression in the adult rat brain at high resolution, we performed fluorescence in situ hybridization (FISH) with specific probes. Confocal images of the CA3 hippocampal field showed that CD44 mRNA expression overlapped with immunostaining of the neuronal marker MAP-2 (Figure 1A). The sense probe of CD44 mRNA was used as a negative control to confirm the specificity of the FISH results. To further explore the subcellular distribution of CD44, we used immunogold labeling in the adult rat hippocampus. Immunogold particles were frequently associated with asymmetric synapses (Figure 1B). Of interest, CD44 labeling in the CA3 stratum radiatum was detected at both presynaptic and postsynaptic sites. The quantitative analysis of the number of gold particles in dendritic spines and axonal boutons confirmed a significant association between gold particles and these compartments compared with an expected random distribution (dendritic spines: $\chi^2 = 1140.37$, $p < 0.00001$; axonal boutons: $\chi^2 = 217.739$, $p < 0.00001$). For the negative control, the primary antibody was replaced with nonimmune immunoglobulin G (IgG). In this case, the distribution of gold particles within the synapses did not significantly differ from the random distribution (dendritic spines: $\chi^2 = 0.08$, $p > 0.05$; presynaptic sites: $\chi^2 = 2.45$, $p > 0.05$). These data clearly indicate the synaptic localization of CD44 at spiny excitatory sites in mature hippocampal neurons. In addition to the synaptic localization of CD44, immunogold staining also confirmed the presence of CD44 in astrocytes (unpublished data; Supplemental Figure S1).

CD44 regulates dendritic spine morphology

The expression of synaptic CAMs is crucial for proper synapse maintenance and dendritic spine structure (Kasai *et al.*, 2003; Dalva *et al.*, 2007; Koleske, 2013). Therefore we tested whether CD44 regulates spine morphology. We recently demonstrated the high knockdown efficiency of CD44 shRNA in young primary hippocampal neurons (Skupien *et al.*, 2014) and astrocytes (Konopka *et al.*, 2016). Similarly, we tested the efficacy of CD44 knockdown in adult cultured neuronal cells. Endogenous CD44 was detected at 3-wk-old hippocampal cultures by immunofluorescence, and the intensity of immunostaining was compared. As shown in Figure 2A, CD44 short hairpin RNA (shRNA) significantly decreased the level of endogenous protein. Next we examined the effects of CD44 knockdown on spine shape in cultured hippocampal neurons. Cells on 14 d in vitro (DIV) were transfected with a pSuper plasmid (control) or CD44 shRNA plasmid together with green fluorescent protein (GFP)–encoding vector. Cotransfection with a GFP-encoding plasmid enabled the visualization of dendritic spines (Figure 2B). The data were collected from three separate experiments and normalized to controls. An extensive morphological analysis of >3000 dendritic spines that was performed on 21 DIV revealed that the spines of CD44 shRNA–transfected cells exhibited an increase in length (pSuper, 1.00 ± 0.005 µm; CD44 shRNA, 1.06 ± 0.008 µm; $p = 0.005$; Figure 2B), and their head width was significantly reduced (pSuper, 1.00 ± 0.005 µm; CD44 shRNA, 0.935 ± 0.006 µm; $p < 0.0001$; Figure 2C). Total spine density was not significantly different between groups (pSuper, 0.98 ± 0.02 spines per 1 µm of dendrite; CD44 shRNA, 0.94 ± 0.02 spines per 1 µm of dendrite; Figure 2D). To confirm the specificity of the observed CD44-knockdown phenotype, we performed rescue experiments. We used a DNA construct in which silent mutations were introduced into the cDNA that encoded rat CD44 (CD44Rescue) that was transcribed into mRNA, which could not be recognized by shRNA. We recently showed that the coexpression of CD44Rescue with shRNA in neurons resulted in the reexpression of CD44 at endogenous levels (Skupien *et al.*, 2014). After the coexpression of CD44shRNA together with CD44Rescue, we observed a reversal of the following knockdown-induced phenotypes: length (pSuper, 1.00 ± 0.01 µm; CD44 shRNA, 1.068 ± 0.01 µm; CD44Rescue, 1.03 ± 0.02 µm; pSuper/CD44 shRNA, $p < 0.0001$; pSuper/CD44Rescue, $p = 0.07$; CD44 shRNA/CD44Rescue, $p = 0.01$) and head width (pSuper, 1.00 ± 0.01 µm; CD44 shRNA, 0.84 ± 0.01 µm; CD44Rescue, 0.975 ± 0.02 µm; pSuper/CD44 shRNA, $p < 0.0001$; pSuper/CD44Rescue, $p = 0.21$; CD44 shRNA/CD44Rescue, $p < 0.0001$; Figure 2E). These data indicate that CD44 shRNA-induced changes in dendritic spine morphology resulted from the specific knockdown of CD44 rather than off-target effects.

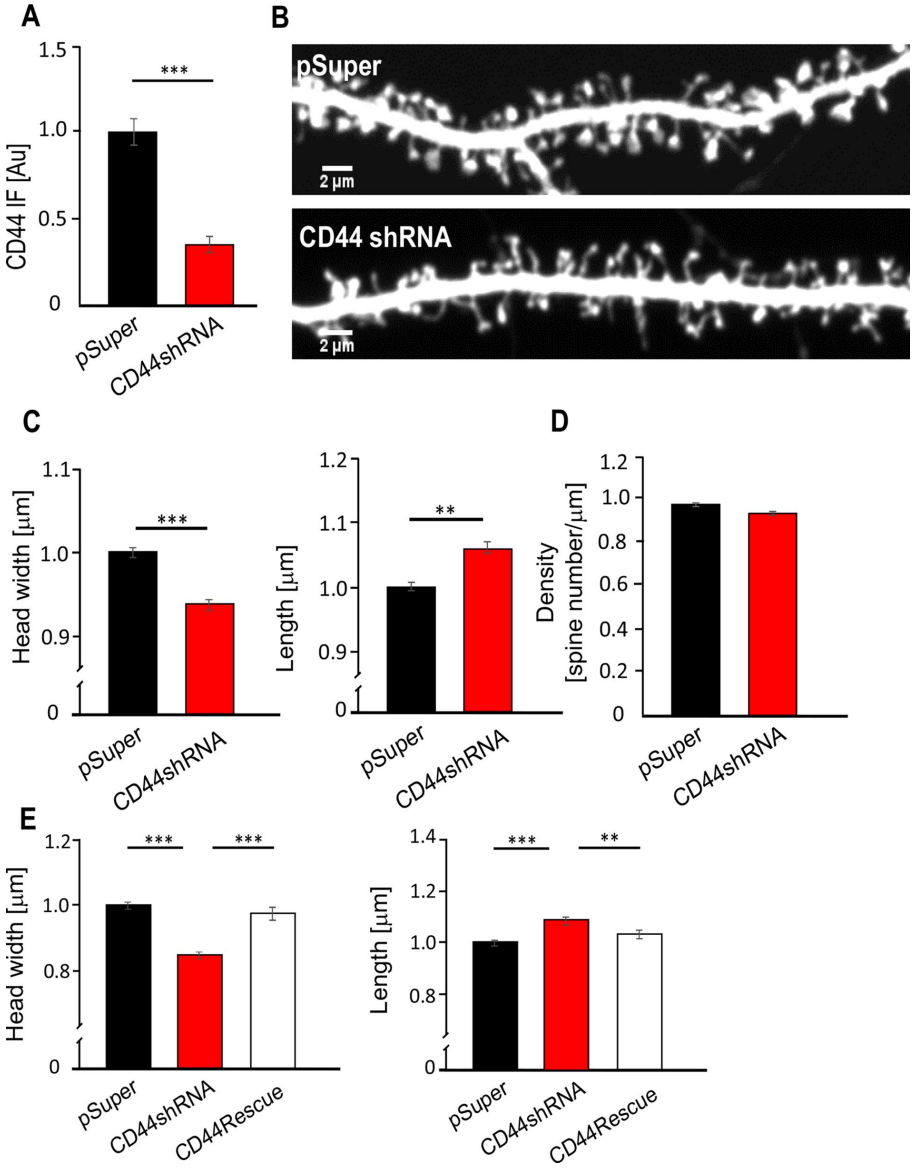

FIGURE 2: CD44 affects dendritic spine morphology. Primary hippocampal neurons transfected with pSuper or CD44 shRNA plasmids together with β-actin–GFP were subjected to immunocytochemistry using anti-CD44 antibody. (A) The effect of CD44 knockdown was estimated based on the average intensity of the CD44 immunofluorescence (IF) signal in transfected cells. AU, arbitrary units; 30 neurons per group. (B) Representative images of dendrites from dissociated hippocampal neurons (on 21 DIV) transfected with pSuper or CD44 shRNA plasmid together with a GFP-encoding vector. Scale bar, 2 µm. (C) Analysis of dendritic spine head width (left) and length (right) in all three groups. (D) Analysis of dendritic spine density. (E) Analysis of dendritic spine head width (left) and length (right) of cells cotransfected with pSuper, CD44 shRNA, or CD44 shRNA/CD44Rescue together with a GFP-encoding vector. The data were obtained from 25–30 neurons per group in three independent cultures, pSuper $n_{spines} = 4409$, CD44 shRNA $n_{spines} = 3578$. The "rescue" experiment pSuper $n_{spines} = 450$, CD44 shRNA $n_{spines} = 500$, and CD44 shRNA/CD44Rescue $n_{spines} = 350$. The data are expressed as mean ± SEM. $^{**}p < 0.01$, $^{***}p < 0.001$ (Student's *t* test).

Impaired excitatory synaptic transmission in hippocampal neurons with CD44 knockdown

The electrophysiological properties of synapses are tightly associated with changes in dendritic spine morphology and synaptic

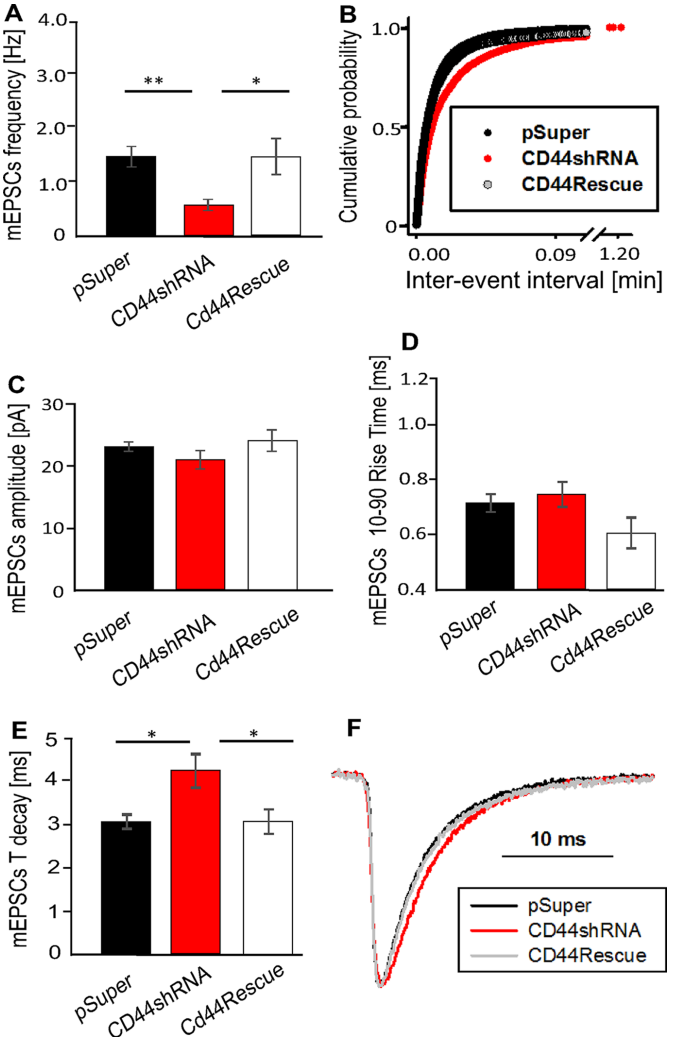

FIGURE 3: Single neurons transfected with CD44 shRNA construct in wild-type cultures exhibit a significant deficit in AMPA/kainate receptor glutamatergic transmission. (A–F) Statistics for standard parameters of AMPA/kainate mEPSCs recorded in control neurons (black), CD44 shRNA (red), and CD44Rescue neurons (white). (A) The average mEPSC frequency recorded in CD44shRNA neurons was significantly smaller than with control and CD44Rescue cells. (B) Cumulative plots of the time interval between subsequent mEPSCs recorded in various neurons. Note that CD44 silencing resulted in significant prolongation of the occurrence of mEPSCs (red line). (C, D) The manipulation of CD44 expression did not result in a significant alteration of mEPSC amplitude and 10–90 rise time. (E) Statistics of the average mEPSC monoexponential decay time constant (τ). CD44 knockdown neurons exhibited significantly larger τ values than with control and CD44Rescue cells. (F) Example of averaged mEPSC traces obtained from control neurons (black line), CD44 shRNA neurons (red line), and CD44Rescue neurons (gray line). Note the prolonged decay of mEPSCs recorded in CD44-knockdown neurons. The data were obtained from 8–13 neurons per group. The data are expressed as mean ± SEM. *$p < 0.5$, **$p < 0.01$ (Student's *t* test).

plasticity (Kasai *et al.*, 2003; Noguchi *et al.*, 2011; Sala and Segal, 2014; Tonnesen *et al.*, 2014). Moreover, the vast majority of excitatory synapses are localized at dendritic spines (Bourne and Harris, 2008), and most of them are glutamatergic. Different adhesion molecules have been implicated in the regulation of synaptic plasticity and signal transmission between neurons (Dalva *et al.*, 2007; Wlodarczyk *et al.*, 2011; Conant *et al.*, 2015). To determine the potential functional consequences of lower CD44 expression in the postsynaptic cell, we performed electrophysiological experiments using hippocampal pyramidal neurons in culture that were cotransfected at 14 DIV with a noncoding pSuper plasmid (control) or CD44 shRNA plasmid together with a GFP-encoding vector to allow cell visualization. Patch-clamp, single-cell recordings were performed at 18–21 DIV. Only cells that exhibited green fluorescence were examined. We recorded miniature excitatory postsynaptic currents (mEPSCs) that were mediated by α-amino-3-hydroxy-5-methyl-4-isoxazolepropionic acid (AMPA)/kainate receptors. We found that the average frequency of mEPSCs in CD44-knockdown neurons (Figure 3A) significantly decreased (CD44 shRNA, 0.5 ± 0.1 Hz, n = 12) compared with the control (pSuper, 1.4 ± 0.2 Hz, n = 13, p = 0.001). This difference was also visualized by analyzing the cumulative distributions of interevent intervals for individually recorded mEPSCs and exemplary averaged mEPSC traces (Figure 3, B and F). We then analyzed the mEPSC characteristics in more detail. Of interest, the manipulation of CD44 expression did not significantly change the average mEPSC amplitude (pSuper, 22.8 ± 0.9 pA, n = 13; CD44 shRNA, 21 ± 1 pA, n = 13, p = 0.26) or the 10–90% mEPSC rise time (pSuper, 0.71 ± 0.04 ms, n = 12; CD44 shRNA, 0.74 ± 0.05 ms, n = 12, p = 0.63; Figure 3, C and D). However, the average mEPSC deactivation constant (τ_{decay}) that was recorded in CD44-knockdown cells (CD44 shRNA, 4.5 ± 0.2 ms, n = 11) significantly increased compared with control cells (pSuper, 4.0 ± 0.1 ms, n = 12, p = 0.03; Figure 3E). Similar to the previous experiment, we used CD44Rescue construct to confirm the specificity of obtained results. The coexpression of CD44shRNA together with CD44Rescue plasmid resulted in the reversal of the knockdown-induced changes in the average mEPSC frequency (CD44Rescue, 1.4 ± 0.4 Hz, n = 8; pSuper/CD44Rescue p = 0.97; CD44Rescue/CD44 shRNA p = 0.04) and average mEPSC deactivation constant (τ_{decay}; CD44Rescue, 4.0 ± 0.1 ms, n = 8; pSuper/CD44Rescue p = 0.99; CD44Rescue/CD44 shRNA p = 0.04). Moreover, we did not observe significant changes in the average mEPSC amplitude (CD44Rescue, 23.86 ± 1.8 pA, n = 8; pSuper/CD44Rescue p = 0.6; CD44Rescue/CD44 shRNA p = 0.2) or the 10–90% mEPSC rise time (CD44Rescue, 0.6 ± 0.06 ms, n = 8; pSuper/CD44Rescue p = 0.1; CD44Rescue/CD44 shRNA p = 0.1) between analyzed groups. Thus the observed changes can be attributed to the specific effect of protein down-regulation. Altogether, CD44 knockdown resulted in a pronounced reduction of the number of excitatory synaptic events and prolonged current decay.

CD44 knockdown affects the number of presynaptic boutons, as revealed by coimmunostaining of Bassoon and PSD-95

The changes in the frequency of mEPSCs that we observed upon CD44 knockdown in hippocampal neurons may be a result of an alteration in the number of functional synapses. Therefore we examined synapses of neurons that were transfected with pSuper or CD44 shRNA plasmids by immunostaining the postsynaptic protein PSD-95 and presynaptic marker Bassoon (Figure 4A; Lanore *et al.*, 2010). First, we measured the average PSD-95 immunostaining intensity within dendritic spines relative to the fluorescence intensity in dendritic shaft. The fluorescence intensity of PSD-95 was lower in neurons with reduced CD44 expression (CD44 shRNA, 2.21 ± 0.05; Figure 4B) than in control cells (pSuper, 2.98 ± 0.09, $p < 0.0001$). To quantify the number of synapses that were located on the surface of individual dendrites, we counted the number of Bassoon-positive puncta on three-dimensional reconstructions of selected dendritic segments using Imaris software as described

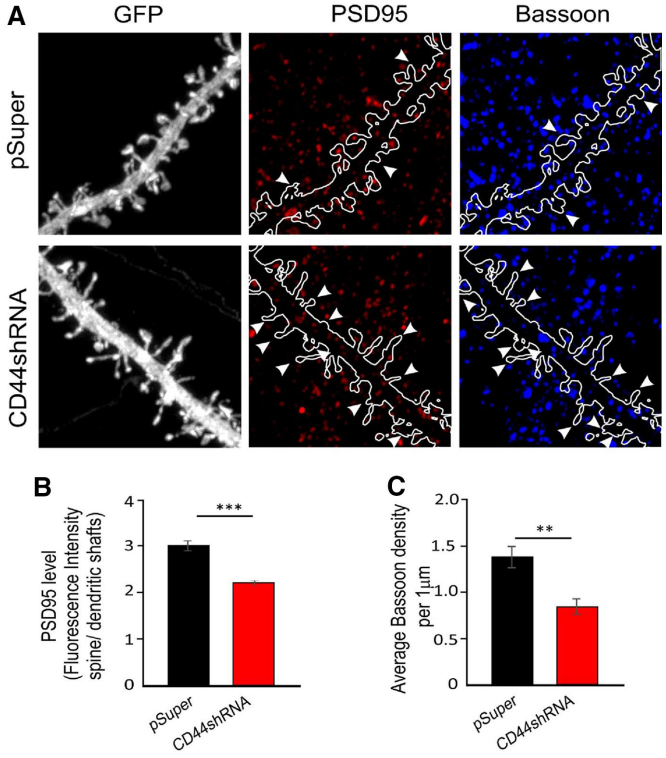

FIGURE 4: CD44 shRNA reduces the number of Bassoon-positive presynaptic puncta. (A) Representative images of dendritic segments of pSuper- or CD44 shRNA-transfected cells immunostained with anti-Bassoon and anti–PSD-95 antibodies. Arrowheads indicate dendritic spines with decreased PSD-95 level or without Bassoon signal. (B) Analysis of average PSD-95 fluorescence intensity within dendritic spines vs. dendritic shafts. (C) Quantification of average density of Bassoon-positive puncta localized within 0.2 µm of the neuronal surface apposed to the dendritic spine. The data were obtained from 8–10 neurons per group, pSuper $n_{spines} = 600$ and CD44 shRNA $n_{spines} = 700$ in three separate experiments. The data are expressed as mean ± SEM. $^{**}p < 0.01$, $^{***}p < 0.001$ (Student's *t* test).

previously (Fogarty *et al.*, 2013). Such an approach increases the accuracy of immunolabeling analysis and eliminates the fluorescence signal from surrounding cells. The quantification of Bassoon puncta within 0.25 µm from the spine surface revealed a decrease in the average density of Bassoon puncta that were closely apposed to the dendritic spines in CD44 shRNA–transfected neurons (CD44 shRNA, 0.84 ± 0.08; Figure 4C) compared with the control (pSuper, 1.39 ± 0.12, $p = 0.002$), which is consistent with the observed decrease in the frequency of mEPSCs in CD44-knockdown cells. These results suggest that the number of functional synapses is reduced after silencing CD44 expression.

Activity-dependent structural plasticity of dendritic spines is regulated by CD44

The structural flexibility of dendritic spines enables the dynamic remodeling of neuronal contacts, changing the way in which the neuronal circuit processes information (Yuste and Bonhoeffer, 2001). The aforementioned results imply that CD44 expression plays a crucial role in proper synaptic function. To determine whether CD44 also contributes to activity-dependent plastic changes in dendritic spine structure, we performed live-cell imaging experiments in which we induced chemical long-term potentiation (cLTP) through the bath application of a forskolin/rolipram/picrotoxin mixture. Such treatment has been shown to result in the long-lasting enhancement of neuronal activity and the remodeling of dendritic spine shape (Otmakhov *et al.*, 2004; Szepesi *et al.*, 2013, 2014). To investigate the influence of CD44 expression on cLTP-induced changes in spine morphology, we imaged dendritic fragments of cells that were transfected with pSuper or CD44 shRNA plasmids under a confocal microscope before and 40 min after cLTP induction. The same spines were identified at both time points. Next we calculated relative changes (see *Materials and Methods* for details) in the dendritic spine head width of each identified spine. Representative dendritic segments of neurons that were cotransfected with a GFP-encoding vector and the noncoding pSuper plasmid (control) or CD44 shRNA are shown in Figure 5A. The detailed morphometric analysis of individual spines that were subjected to cLTP stimulation revealed a robust and a long-lasting increase in the relative spine head width in response to the 40-min stimulation in control cells (pSuper + dimethyl sulfoxide [DMSO], 0.02 ± 0.02; pSuper + cLTP, 0.11 ± 0.014, $p < 0.0001$; Figure 5B), whereas spine head expansion was completely inhibited in CD44 shRNA cells (CD44 shRNA + DMSO, 0.03 ± 0.02; CD44 shRNA + cLTP, 0.02 ± 0.02, $p = 0.4949$; Figure 5B). These data indicate that CD44 expression is crucial for plastic changes in dendritic spines upon stimulation.

CD44 regulates the activity of small Rho GTPases in dendritic spines of hippocampal neurons

Numerous structural and functional changes in dendritic spines have been shown to be strictly determined by the highly dynamic actin cytoskeleton, the architecture of which is modulated through several signaling pathways (Ethell and Pasquale, 2005; Tada and Sheng, 2006; Chen *et al.*, 2007). Among the well-known actin regulators is the Rho family of GTPases (Cdc42, RhoA, Rac1), which are also implicated in the morphogenesis of dendritic spines (Hall and Nobes, 2000; Tashiro *et al.*, 2000; Saneyoshi *et al.*, 2010) through their modulatory effects on spinoskeletal organization (Hotulainen and Hoogenraad, 2010). In addition, CD44 regulates RhoA, Cdc42, and Rac1 activity by interacting with the regulatory GTPase-activating proteins (GAPs) and guanine nucleotide exchange factors (GEFs) in tumor cells (Bourguignon *et al.*, 2000, 2001, 2003, 2005). We used Raichu-RhoA, Raichu-Rac1, and Raichu-Cdc42 FRET-based biosensors (Itoh *et al.*, 2002; Yoshizaki *et al.*, 2003) to determine whether alterations in the expression of CD44 are accompanied by changes in RhoA, Rac1, and Cdc42 activity in neuronal cells (Figure 6A). Neurons were cotransfected with Raichu-RhoA, Raichu-Rac1, or Raichu-Cdc42 together with the noncoding pSuper plasmid (control) or CD44 shRNA plasmid (Figure 6, B–D). The occurrence of FRET between fluorophore molecules (donor cyan fluorescent protein [CFP] and acceptor yellow fluorescent protein [YFP]) in each Raichu probe reflects GTPase activation and is revealed by a shortened average donor fluorescence lifetime. We analyzed the averaged fluorescence lifetime of the donor molecule (CFP) using time-correlated single-photon counting fluorescence lifetime imaging microscopy (Figure 6, B–D) within the dendritic spines as described in *Materials and Methods*. In this assay, the silencing of CD44 expression affected the level of activity of all three GTPases (RhoA, Rac1, and Cdc42). Fluorescence resonance energy transfer between the donor and acceptor affects donor fluorescence decay and leads to a shortened donor lifetime upon Rho GTPase activation, whereas an increase in donor lifetime indicates that the activity of the protein and FRET decrease. The average fluorescence lifetime of the donor fluorophore of the Raichu-Cdc42 probe for CD44-depleted cells was significantly shortened compared with control cells (pSuper, 3.15 ± 0.15 ns; CD44 shRNA, 2.37 ± 0.12 ns; $p = 0.006$;

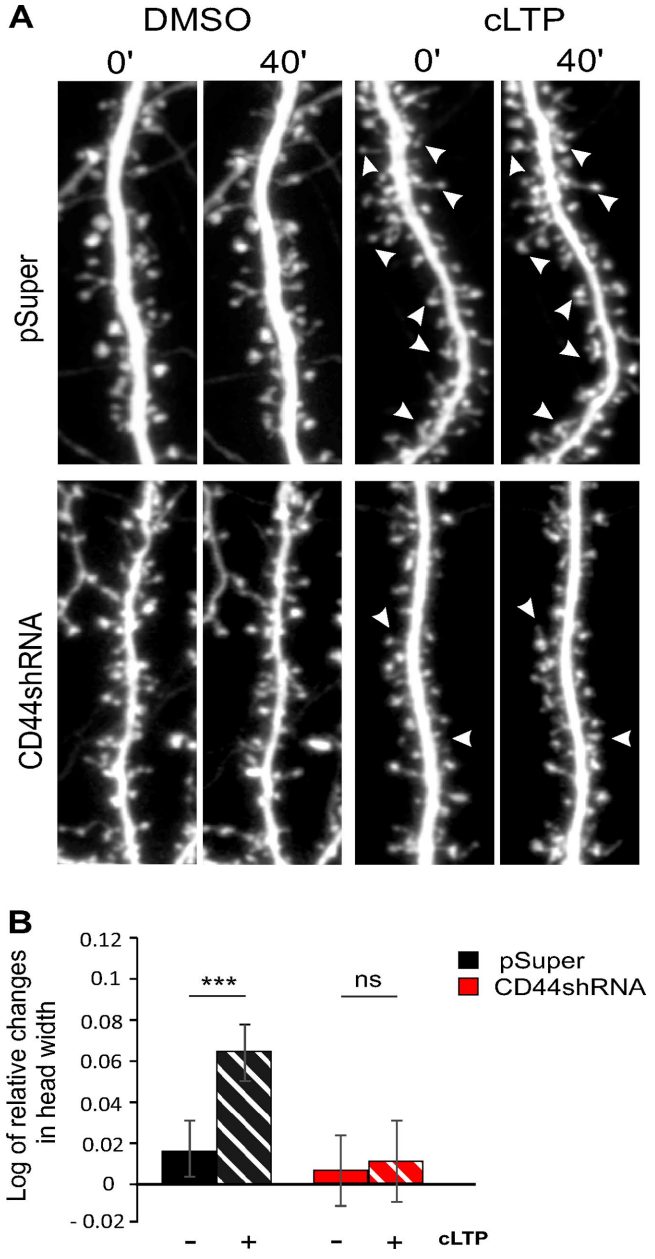

FIGURE 5: Activity-dependent structural plasticity of dendritic spines is regulated by CD44. Live-imaging sessions of neurons cotransfected with pSuper or CD44 shRNA plasmid together with a GFP-encoding vector were performed under control conditions (DMSO) and 40 min after cLTP induction. Arrowheads indicate examples of dendritic spines that increased upon cLTP induction. (A) Representative images of dendritic segments captured during the live-imaging experiment under control (DMSO) and cLTP-stimulated conditions (indicated by minus and plus signs, respectively). Open bars, cells treated with DMSO; hatched bars, cells stimulated with cLTP mixture. (B) Graph representing relative changes in the spine head width. The data were obtained from 8–10 neurons per condition, pSuper + DMSO n_{spines} = 420, pSuper + cLTP n_{spines} = 700, CD44 shRNA + DMSO n_{spines} = 400, and CD44 shRNA n_{spines} = 478. The data are expressed as mean ± SEM. ***$p < 0.001$ (Student's *t* test).

Figure 6B). A similar effect was observed for cells cotransfected with the Raichu-Rac1 probe (pSuper, 3.15 ± 0.04 ns; CD44 shRNA, 2.7 ± 0.03 ns; $p < 0.0001$; Figure 6C). This demonstrates higher levels of Cdc42 and Rac1 activation in dendritic spines of CD44-depleted cells. In contrast, we observed a longer mean fluorescence lifetime of the donor fluorophore of the Raichu-RhoA probe in CD44-knockdown cells than in control neurons (pSuper, 3.04 ± 0.07 ns; CD44 shRNA, 3.87 ± 0.1 ns; $p < 0.0001$; Figure 6D), implying a lower level of activation of RhoA in neurons with reduced CD44 expression.

To determine whether the function of CD44 in regulating dendritic spine morphology is driven by changes in Cdc42 activity, we expressed a dominant-negative (DN) form of Cdc42 together with the CD44 shRNA vector (Figure 6, E–G). We found that the expression of DN-Cdc42 rescued CD44 shRNA-induced dendritic spine elongation (pSuper, 1.00 ± 0.01; CD44 shRNA, 1.07 ± 0.02; CD44 shRNA_DN-Cdc42, 1.01 ± 0.01; pSuper/CD44 shRNA, $p = 0.0007$; pSuper/CD44 shRNA_DN-Cdc42, $p = 0.76$; CD44 shRNA/CD44 shRNA_DN-Cdc42, 0.003; Figure 6F). Moreover, the CD44 shRNA-induced decrease in spine head width was also partially rescued by DN-Cdc42 expression (pSuper, 1 ± 0.01; CD44 shRNA, 0.83 ± 0.01; CD44 shRNA_DN-Cdc42, 0.88 ± 0.01; pSuper/CD44 shRNA, $p < 0.0001$; pSuper/CD44 shRNA_DN-Cdc42, $p < 0.0001$; CD44 shRNA/CD44 shRNA_DN-Cdc42, $p = 0.0004$; Figure 6G). We performed a rescue experiment using DN-Cdc42 because the activity of this GTPase mutant was previously shown to have no clear effects on dendritic spine length and density (Tashiro *et al.*, 2000), in contrast to the DN form of Rac1 or the constitutively active (CA) form of RhoA. The expression of Rac1-DN, and RhoA-CA was previously shown to disrupt dendritic spine morphology and negatively affect spine density (Nakayama *et al.*, 2000; Tashiro *et al.*, 2000). Similarly, in our experiments, DN-Cdc42 plasmid did not induce changes in dendritic spine length in comparison to control neurons (pSuper_DN-Cdc42, 0.97 ± 0.8, $p = 0.1$). In contrast, pSuper_DN-Cdc42 transfected cells exhibited significant reduction in dendritic spine head width (0.76 ± 0.01) compared with other analyzed groups (pSuper/pSuper_DN-Cdc42, $p < 0.0001$; CD44 shRNA/pSuper_DN-Cdc42, $p = 0.001$; CD44shRNA_DN-Cdc42/pSuper_DN-Cdc42, $p < 0.0001$). A similar effect—a reduction in the number of mushroom-shaped spines—was reported by others (Jausoro *et al.*, 2013; Vadodaria *et al.*, 2013). Our results indicate that CD44 modulates the activity of all three small Rho GTPases. It is involved in RhoA activation and Cdc42 and Rac1 inhibition. By doing so, it modulates dendritic spine morphology.

DISCUSSION

Cell adhesion molecules regulate synaptic transmission and influence dendritic spine structure (Shi and Ethell, 2006; Lonskaya *et al.*, 2013; Ning *et al.*, 2013; Conant *et al.*, 2015). In the present study, we demonstrated the presynaptic and postsynaptic localization of CD44 in the adult brain using sensitive, high-resolution techniques and evaluated the role of CD44 in mature neurons. We found that alterations in CD44 expression modulate the structural and functional properties of the synapse.

The loss-of-function experiments revealed an important role for CD44 in the development and/or maintenance of proper dendritic spine morphology. Filopodia-like dendritic spines are usually considered to be less mature, with a higher potential for "learning" than large, mushroom-type spines (Kasai *et al.*, 2003; Matsuzaki *et al.*, 2004; Bourne and Harris, 2007; Szepesi *et al.*, 2014). Therefore spine elongation and thinning in CD44-depleted cells can indicate their juvenilization. The lower level of PSD-95 in dendritic spines observed upon CD44 knockdown may also explain such a "less mature" phenotype because PSD-95 has been shown to promote synaptic maturation and stabilization (Taft and Turrigiano, 2014). Of interest, we observed a decrease in the frequency of AMPA receptor–mediated mEPSCs, together with no changes in mEPSCs amplitude upon CD44

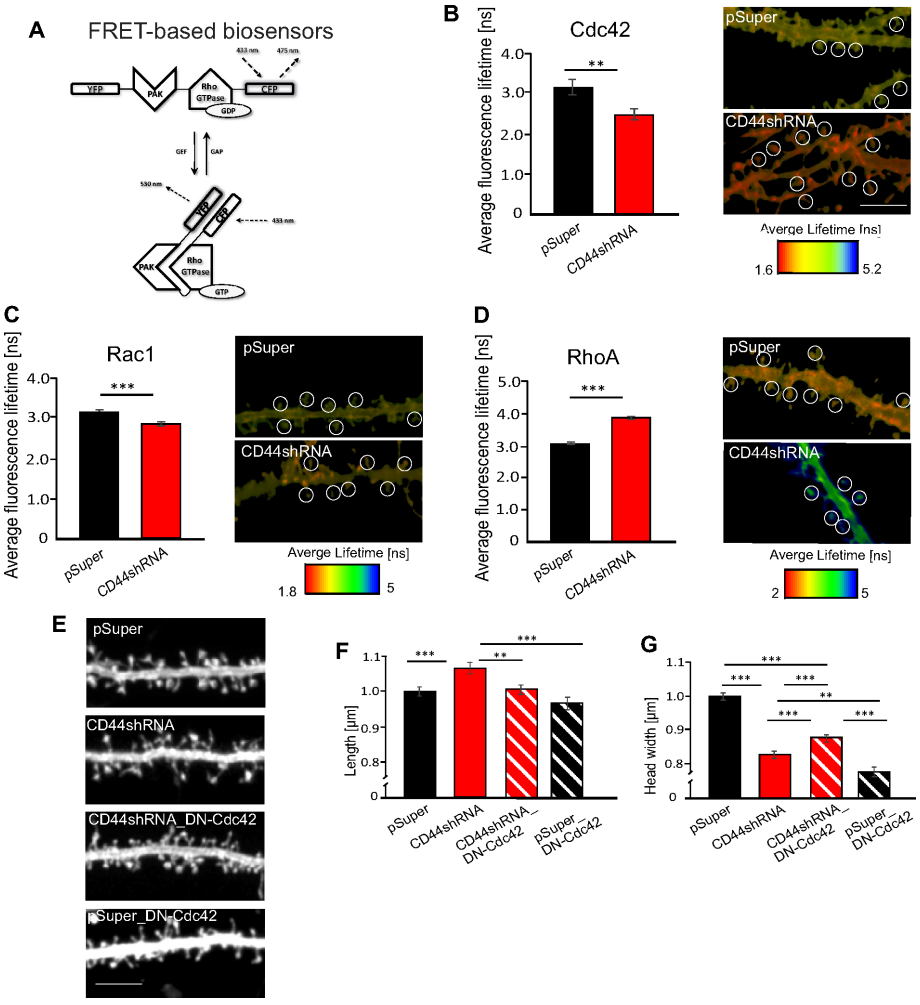

FIGURE 6: CD44 regulates the morphology of dendritic spines by altering the activity of small GTPases RhoA, Rac1, and Cdc42. (A–D) CD44-dependent modulation of activity of small Rho-GTPases (RhoA, Rac1, and Cdc42). (A) Structure of FRET-based biosensors of small Rho GTPase activity. (B–D) Average fluorescence lifetimes for donor (CFP) in dendritic spines of cells cotransfected with pSuper or CD44 shRNA plasmid together with Raichu-Cdc42 (B), Raichu-Rac1 (C), or Raichu-RhoA (D) FRET sensor, with representative fluorescence lifetime images of all analyzed groups. Scale bar, 5 µm. The corresponding color histograms depict the lifetime distribution in a false color scheme and visualize the lifetime variations. Warmer colors indicate shorter lifetimes and a higher level of activated protein. Cooler colors indicate longer lifetimes and a lower level of small Rho GTPase activity. (E–G) Defects in dendritic spine morphology that were induced by CD44 knockdown were rescued by the inhibition of Cdc42 activity. (E) Representative images of dendrites from dissociated hippocampal neurons (on 21 DIV) transfected with pSuper, CD44 shRNA, CD44 shRNA_DN-Cdc42, and pSuper_DN-Cdc42 plasmids together with a GFP-encoding vector. Scale bar, 5 µm. Analysis of dendritic spine length (F) and head width (G) in all four groups. The lifetime data were collected from 8–10 neurons per group and an average of 100 spines per group. The morphological data were obtained from 10–15 neurons per group and an average of 600 spines per group. The data are expressed as mean ± SEM. $^{**}p < 0.01$, $^{***}p < 0.001$ (Student's *t* test).

knockdown. These results may also be attributable to disruption of the synaptic level of PSD95, in which similar changes in the frequency but not amplitude of mEPSCs have been observed in PSD95-knockout mice. Of interest, these knockout animals also exhibited an increase in dendritic spine length (Beique *et al.*, 2006).

Modifications in dendritic spine structure are tightly coupled with neuronal function. The significant decrease in the frequency of mEPSCs upon CD44 knockdown (Figure 2A) was consistent with our imaging data, in which CD44 shRNA reduced the density of Bassoon/PSD-95–positive synaptic puncta (Figure 4), which reflects a considerably lower number of functional synapses. This is further supported by the lack of effect of CD44 knockdown on mEPSC amplitude and rise-time kinetics, suggesting no major alterations in the number of postsynaptic receptors (Figure 2, C and D). Consistent with the present data, a previous study showed that hyaluronidase treatment in cultured neurons did not alter the frequency, kinetics, or amplitude of mEPSCs, indicating that no major changes in synaptic transmission occurred after the enzymatic removal of HA (Frischknecht *et al.*, 2009). CD44 is present in both presynaptic and postsynaptic compartments in vivo, and it would be interesting to determine the primary site that was affected by our manipulation of CD44 expression in culture. Measurements of synaptic currents were performed in transfected cells that should be regarded as postsynaptic. However, we cannot completely exclude the possibility that modifications occurred at the presynaptic compartment. Changes in CD44 expression on the postsynaptic membrane may affect the presynaptic part through retrograde signaling that is triggered by shedding the CD44 extracellular domain by extracellular proteases (Chetty *et al.*, 2012). The cleavage of other synaptic adhesion molecules was previously shown to occur at synapses and be implicated in a reduction of synaptic transmission (Peixoto *et al.*, 2012; Conant *et al.*, 2015). Moreover, CD44 that is localized at postsynaptic sites may also influence the local concentrations of CD44-binding ligands (e.g., cytokines, proteases, other receptors) in the synaptic cleft, thereby modulating synaptic function.

Of interest, CD44 knockdown had no effect on mEPSC rise-time kinetics, but it resulted in a small (0.4 ms) but consistent prolongation of mEPSC decay (Figure 2, E and F). The source of such a subtle change in current kinetics may be attributable to significantly longer spines upon CD44 manipulation (Figure 3B), higher spine neck resistance, and the filtering of synaptic currents, or changes in diffusion of the neurotransmitter in the synaptic cleft, thus contributing to alterations in glutamate transients. Both scenarios were previously implicated in the functional change in the time course of synaptic currents (mEPSC decay kinetics; Barbour *et al.*, 1994; Cathala *et al.*, 2005; Michaluk *et al.*, 2011). More detailed investigations are necessary to elucidate this issue.

Extracellular matrix components and receptors have been implicated in regulating the development and structural modifications of dendritic spines (for extensive review, see Dansie and Ethell, 2011; Wlodarczyk *et al.*, 2011; Levy *et al.*, 2014; Conant *et al.*, 2015). The lack of CD44 might reduce binding to extracellular HA, thus affecting

the stabilization of mature dendritic spines provided by the ECM (Levy *et al.*, 2014). The importance of CD44-mediated cellular interactions with the ECM is further emphasized by a study that showed that HA modulates hippocampal synaptic plasticity, in which the enzymatic removal of hyaluronan disrupted L-type voltage-dependent Ca^{2+} channel–mediated Ca^{2+} transients and LTP (Kochlamazashvili *et al.*, 2010).

Alternatively, CD44-dependent morphological and functional effects can occur as a result of triggering specific intracellular signaling pathways. CD44 binds and regulates the activity of different intracellular ligands. CD44 can influence Rho GTPase activity through interactions with regulatory GEFs and GAPs (Ponta *et al.*, 2003; Bourguignon, 2008). The binding of CD44 to hyaluronan inhibits Cdc42 activity through interactions with IQGAP1 protein in cancer cells (Bourguignon *et al.*, 2005). In contrast, the CD44–HA interaction is known to stimulate the RhoA-mediated signaling pathway and Rho kinase activation through interactions with the RhoA-specific GEF p115Rho (Bourguignon *et al.*, 2003). CD44 also modulates the activity of Rac1 by the Vav2 molecule in nonneuronal cells (Bourguignon *et al.*, 2001). The activity of all three small Rho GTPases has been shown to control dendritic spine formation, stability, and structure (Sala and Segal, 2014). An emerging general view suggests that Rac1 and Cdc42 stimulate dendritic spine growth and stability (Meng *et al.*, 2002; Hotulainen *et al.*, 2009), whereas RhoA inhibits these processes and leads to dendritic spine loss (Tashiro *et al.*, 2000). However, several studies that reported contradictory results suggest that such a conclusion might be too simplistic (Sala and Segal, 2014). Instead, proper dendritic spine maintenance requires an optimal level of small Rho GTPase activation. CD44 depletion altered the activity of Rac1, RhoA, and Cdc42 and impaired spine morphology (i.e., longer and thinner spines). The findings that have been reported by different groups are consistent with our observations, in which the active form of Rac1 resulted in the presence of long, filopodia-like extensions (Nakayama *et al.*, 2000), whereas the inhibition of RhoA dramatically increased the length of spine necks (Tashiro *et al.*, 2000). Of interest, Tashiro and Yuste (2004) proposed that the action of Rac1 is crucial for spine head growth and stabilization, whereas RhoA/Rho kinase is responsible for the conversion of dynamic, long filopodia into stable spines. These observations suggest the existence of a balance between Rac1 and RhoA activity with regard to proper dendritic spine morphology. In addition, we found that the loss of Cdc42 function restored the average length of dendritic spines in neurons with lower CD44 expression, suggesting that optimal level of Cdc42 activity within dendritic spines is responsible for their elongation. Of interest, the dendritic spine head width was only partially rescued by inhibiting Cdc42 activity, indicating that two other GTPases (Rac1 and/or RhoA), in addition to Cdc42, may be involved in the CD44-driven regulation of dendritic spine head size. Cdc42 is a well-known regulator of filopodia formation in different cell types (Shi and Ethell, 2006). The local and rapid activation of Cdc42 also regulates dendritic spine structure, which is indispensable for spine formation and plasticity (Barbour *et al.*, 1994; Tashiro *et al.*, 2000; Hotulainen *et al.*, 2009), but several discrepancies have been found among studies. Contrary to our results, one hypothesis is that Cdc42 activity may be important for spine head expansion (Hotulainen *et al.*, 2009). However, the acquisition of proper spine morphology strictly depends on the time course and localization of Cdc42 activity and other Rho GTPases (Murakoshi *et al.*, 2011). Moreover, in our model, activity was measured in dendritic spines 7 d after transfection with the CD44 shRNA plasmid. Therefore we can assume that changes in CD44 expression resulted in prolonged (days) disruption of the activity of Rac1, RhoA, and Cdc42 within dendritic spines.

In addition, with regard to steady-state morphological and functional changes of spines, we found that the activity-dependent structural plasticity of dendritic spines is CD44 dependent. Structural plasticity that occurs upon the induction of LTP is associated with dendritic spine enlargement (Matsuzaki *et al.*, 2004; Kopec *et al.*, 2006; Yang *et al.*, 2008). Using cLTP that mimics several LTP aspects, we potentiated synapses and confirmed the spine head growth in control cells shown by Szepesi *et al.* (2014). Such an effect was completely abolished in neurons that exhibited a decrease in CD44 expression. The lack of spine head growth upon cLTP induction may be a consequence of a reduction of PSD-95 levels, in which this postsynaptic protein is responsible for the activity-driven stabilization of morphological changes in dendritic spines (Ehrlich *et al.*, 2007). The abrogation of spine head expansion during cLTP stimulation may also result from a disruption of the activity of the Rho GTPases. A lack of CD44 inhibits RhoA activity, thus blocking initial spine head growth upon stimulation (Murakoshi *et al.*, 2011). The blockade of this pathway, therefore, can disrupt subsequent Cdc42 actions that are involved in spine head expansion (Murakoshi *et al.*, 2011), even though CD44 knockdown results in the continuous activation of Cdc42. Moreover, activation of the Rho signaling pathway is believed to disassemble the actin-based spinoskeleton to allow its further growth and restabilization in an enlarged form (Murakoshi and Yasuda, 2012). Our results are further supported by the fact that the action of RhoA is required for the initial induction of LTP, whereas the Rac1-dependent pathway is required for later LTP consolidation (Rex *et al.*, 2009). Again, CD44 knockdown impaired the first step in the coordinated cross-talk between GTPases and affected activity-dependent changes in spine morphology. Taken together, the present data suggest that the abnormal structure and plasticity of dendritic spines upon the manipulation of CD44 expression may be a consequence of an imbalance in the activity of these three small Rho GTPases. Proper dendritic spine formation, maintenance, and function appear to depend on the coordinated action of all three Rho GTPases. However, we cannot exclude the possibility that other intracellular signaling molecules are also associated with the morphological abnormalities described here.

Cell–ECM interactions are dynamically regulated, and the fact that plastic changes after cLTP stimulation were not found in CD44-depleted cells suggests that CD44 expression levels are tightly regulated to ensure proper synaptic function. Moreover, the contribution of the ECM or its receptors to the modulation of synaptic function has been highlighted in different molecular, behavioral, and cognitive studies. The enzymatic removal of HA has been shown to impair contextual fear conditioning (Kochlamazashvili *et al.*, 2010). The abnormalities in spine morphology that we observed in the present study may underlie learning deficits in CD44-knockout mice (Raber *et al.*, 2014). We propose that the CD44 adhesion molecule plays a critical, multifactorial role in maintaining proper synaptic architecture and function and participates in synaptic plasticity.

MATERIALS AND METHODS

Animal studies

All procedures were performed according to the rules established by the First Local Ethical Committee on Animal Research in Warsaw, based on national laws that are in full agreement with the European Union directive on animal experimentation.

In situ hybridization

FISH was performed according to the procedure described previously (Konopacki *et al.*, 2007). Staining was performed on 40-µm-thick, free-floating sections using fluorescein-labeled cRNA probes for CD44 that were complementary to the full-length CDS of rat CD44 cDNA cloned into the pGEM(R)-T Easy Vector System (Promega, Madison, WI) from a rat cDNA that was produced from total rat spleen RNA using real-time PCR and the RevertAid First Strand cDNA Synthesis Kit (Thermo Scientific, Rockford, IL) and the primers 5′-GGCCGCTACAGTATCTCCAGGACTG-3′ and 5′-CCCCCCGGGCACCCCAATCTTCATATCCAC-3′. Probe detection using peroxidase-conjugated anti-fluorescein antibody (Roche**,** Mannheim, Germany) was followed by the red (Cy3) fluorophore-based tyramide signal-amplification system (NEN, Waltham, MA). Subsequent immunofluorescent costaining was performed with anti–MAP-2 antibody (Sigma-Aldrich, St. Louis, MO) and visualized using Alexa 647–conjugated secondary antibody (Invitrogen, Carlsbad, CA) as described previously (Wilczynski *et al.*, 2008).

Immunogold electron microscopy

The procedure was performed in the hippocampal CA3 field from postnatal day 53 (P53) rat brain as described previously (Wilczynski *et al.*, 2008). For immunodetection, sheep polyclonal anti-CD44 (1:50; R&D Systems, Minneapolis, MN) followed by secondary antibodies coupled to 10-nm gold particles was applied (Electron Microscopy Sciences**,** Fort Washington, PA). Nonimmune sheep IgG (BD PharMingen, San Jose, CA) was used as a negative control. Gold particle densities within various ultrastructural compartments were measured on digital micrographs using ImageJ software (National Institutes of Health, Bethesda, MD). The statistical evaluation of the labeling was performed using χ^2 test of observed and expected gold counts over the given compartments (Mayhew and Lucocq, 2008). The data were sampled randomly. At least 200 gold particles at ~10 images from three animals per group were counted.

DNA constructs

The following mammalian expression plasmids were used: pSuper vector (Brummelkamp *et al.*, 2002), β-actin–GFP (Jaworski *et al.*, 2005), CD44 shRNA, CD44-GFP shRNA-resistant form CD44Rescue; (Skupien *et al.*, 2014), and DN-Cdc42 (cdc42-myc N17 pRH5; a generous gift from Anna Akhmanova, Utrecht University, Utrecht, Netherlands).

Cell cultures

Primary rat hippocampal cultures were prepared from P0 rat brains as described previously (Michaluk *et al.*, 2011) and transfected with Lipofectamine 2000 at 14 DIV according to the manufacturer's protocol (Invitrogen).

Electrophysiological recordings and data analysis

All electrophysiological recordings were performed with patch-clamp technique in neuronal cultures at 17 DIV (3 d after transfection). Currents were recorded using a Multiclamp 700B amplifier (Molecular Devices, Axon Instruments, Sunnyvale, CA). Analogue signals were low-pass-filtered with a four-pole Bessel filter at 10 kHz and acquired with a sampling time of 50 µs (20 kHz) using Digidata1440 and pClamp 10.3 software. The extracellular solution was composed of (in mM): 137 NaCl, 5 KCl, 2 $CaCl_2$, 2 $MgCl_2$, 10 glucose, and 10 4-(2-hydroxyethyl)-1-piperazineethanesulfonic acid (HEPES), with the pH adjusted to 7.25 with NaOH. The intracellular solution contained the following (in mM): 116 potassium gluconate, 6 KCl, 2 NaCl, 20 HEPES, 0.5 ethylene glycol tetraacetic acid, 4 MgATP, 0.3 NaGTP, and 10 sodium phosphocreatine, with the pH adjusted to 7.25 with KOH. mEPSCs were recorded in a whole-cell voltage-clamp configuration at a holding potential of –63 mV (a typical value of membrane potential in recorded neurons in current-clamp mode, not corrected for liquid junction potential) after bath application of 10 µM gabazine and 1 µM tetrodotoxin (TTX). The presence of magnesium (2 mM) in the external saline and the highly negative membrane voltage were expected to eliminate the *N*-methyl-D-aspartate receptor–mediated component of synaptic currents. After the end of recording, 20 µM AMPA/kainate receptor antagonist 6,7-dinitroquinoxaline-2,3-dione was used to confirm the origin of recorded mEPSCs and lack of γ-aminobutyric acid–ergic currents. All of the chemicals were purchased from Sigma-Aldrich (Poznan, Poland), with the exception of TTX, which was provided by Latoxan (Valence, France). All of the experiments were performed at room temperature (23–24°C). The data analysis was performed in a blind manner and independently by two investigators using pClamp 10.3 software (Molecular Devices, Axon Instruments). mEPSCs were analyzed as previously described (Michaluk *et al.*, 2011). Briefly, the mEPSC decay phase was analyzed on averaged traces by fitting the single-exponential function $A(t) = A_{peak} \cdot e^{(-\tau/\tau_{decay})}$, where A is the amplitude and τ_{decay} is the decay time constant. The rate of an activation phase of mEPSCs was estimated as the time from 10–90% of a maximal (peak) amplitude (10–90% rise time). The series resistance (R_s) was estimated from the response to a hyperpolarizing voltage step (–5 mV; Song and Semyanov, 2011) applied every 20 s in fixed-length episode recording mode. Whole-cell recordings in which the series resistance exceeded 15 MΩ or changed by >10% during the recording were excluded from the analysis. The electrophysiological data were obtained from at least eight neurons per group.

Live imaging and cLTP

Cultured hippocampal neurons were transfected on 14 DIV with pSuper or CD44 shRNA plasmids together with a β-actin GFP plasmid, and live-cell imaging was performed on 20–22 DIV. During the imaging session, the cells were kept in an acquisition chamber at a controlled temperature (37°C) and stable CO_2 concentration (5%). Dendrites of interest were imaged for 1–5 min before stimulation, and then cLTP was induced by bath application of a mixture of 50 µM forskolin, 50 µM picrotoxin, and 0.1 µM rolipram (all from Sigma-Aldrich, St. Louis, MO), each dissolved in DMSO in maintenance medium. As controls, cultures were treated with toxin-free solvent (DMSO; Sigma, St. Louis, MO). Dendritic segments that were decorated with spines were imaged 40 min after cLTP induction. Images were acquired using a Carl Zeiss LSM780 confocal microscope with a C-Apochromat 40×/1.2 numerical aperture (NA) water immersion objective using a 488-nm wavelength argon laser at 3% transmission and 70 nm/pixel resolution. A series of *z*-stacks was acquired at each 0.4-µm step.

Immunofluorescence

The procedures were performed in cultured neurons or brain tissue sections as described previously (Skupien *et al.*, 2014). The following primary antibodies were used: sheep anti-CD44 (1:500; R&D Systems), rabbit anti-Bassoon (1:500; Synaptic Systems, Göttingen, Germany), mouse anti–PSD-95 (1:500; Millipore; Darmstadt, Germany), and chicken anti-MAP-2 (1:1000). The following secondary antibodies were used: anti-chicken Alexa Fluor 488, anti-rabbit Alexa 647, and anti-sheep Alexa 555 (all from donkey, diluted 1:500; Abcam, Cambridge, United Kingdom). The analysis of the average fluorescence intensity of CD44 was performed using ImageJ software. The immunostaining intensity in transfected cells was normalized to

the intensity of nontransfected adjacent cells. Thirty neurons per group were analyzed. Data were obtained from three separate experiments.

Fluorescence lifetime analysis of Cdc42/RhoA/Rac1 FRET sensors

The Raichu-RhoA, Raichu-Rac1, and Raichu-Cdc42 FRET sensors (Itoh *et al.*, 2002; Yoshizaki *et al.*, 2003; Aoki and Matsuda, 2009) were kindly provided by the Michiyuki Matsuda laboratory (Department of Pathology and Biology of Diseases, Graduate School of Medicine, Kyoto University). For measurements of the sensors, neuronal cultures were cotransfected with Raichu-RhoA, Raichu-Rac1, or Raichu-Cdc42 FRET sensors with either noncoding pSuper plasmid (control) or CD44 shRNA plasmid at 14 DIV. The cultures were fixed 7 d after cell transfection, and then imaging was performed. Measurement of the fluorescence lifetime of the donor in each FRET sensor was performed using a Picoquant PicoHarp 300 Time-Correlated Single Photon Counting System connected to a Leica Sp8 confocal microscope using a 63× oil immersion objective (NA 1.4). The donor fluorescence (CFP) was excited by a 405-nm pulse diode laser (PDL 800-B) at 40 MHz. The fluorescence intensity was recorded in the wavelength band from 467 to 499 nm to avoid acceptor fluorescence. Typical fluorescence decays were fitted with the resulting sum of one, two, or three exponentials interactively convolved with the instrument response function. The mean fluorescence lifetimes were calculated as the mean values of the fit function. The lifetime analysis was performed using SymPhoTime software (Picoquant, Berlin, Germany). A two-dimensional map (512 × 256 pixels) of the mean lifetime value was generated for the given experimental condition. For each experiment, 8–10 neurons and an average of 100 spines per group were analyzed. Data were obtained from three separate experiments.

Image acquisition and morphological analysis

The analysis of dendritic spine morphology was performed as described previously (Szepesi *et al.*, 2014). The images that were acquired from fixed material and live imaging sessions were processed using ImageJ software and then analyzed semiautomatically using custom-written SpineMagick software (international patent no. WO/2013/021001; https://patentscope.wipo.int/search/en/detail.jsf;jsessionid=4D8A9E4A975B3D44DAC796BC751D05F5.wapp1nA?docId=WO2013021001&recNum=1&maxRec=&office=&prevFilter=&sortOption=&queryString=&tab=PCT+Biblio). The recorded parameters included spine length and head width. The values were normalized to control cells that expressed the pSuper vector. Dendritic spines from secondary and tertiary dendrites were chosen to eliminate possible systematic differences in their morphologies. The data were obtained from at least 25 cells in each group in three independent experiments, resulting in at least 3600 measured dendritic spines for each group.

Live-imaging analysis and the calculation of changes in spine parameters were performed as described previously (Szepesi *et al.*, 2014). Briefly, the same spines were identified on the subsequent acquired images during the live-imaging sessions (before stimulation and 10 and 40 min after stimulation). Relative changes in dendritic spine morphology parameters were calculated and plotted on a logarithmic scale to ensure the proper contribution of the fluctuations to the total measurement. For both conditions (cLTP treatment and DMSO only), dendritic segments of 8–10 neurons in each group (pSuper/CD44 shRNA) were analyzed. Data were obtained from five separate experiments, resulting in 400–600 spines per condition.

For the analysis of presynaptic markers, images of the immunofluorescently labeled cells were acquired on a Zeiss LSM 780 confocal microscope with *z*-stacks of 0.2 µm. Imaris software (Bitplane AG, Zurich, Switzerland) integrated with Matlab algorithms was used for three-dimensional reconstruction and quantification of the number of presynaptic labeled puncta as described previously (Fogarty *et al.*, 2013). Data were obtained from three independent experiments. On average, 13 neurons and 500–600 dendritic spines per group were analyzed.

Data analysis

The results are expressed as means and SEM. The statistical analysis of immunogold labeling was performed using the χ^2 test with regard to the observed and expected gold counts in the given compartments (Mayhew and Lucocq, 2008). For the statistical analysis of the results from the in vitro experiments, we used Student's *t* test or Student's *t* test with Welch's correction, depending on whether the assumption of homogeneity of variance was met. The statistical analyses were performed using Prism 5.0 software (GraphPad, San Diego, CA).

ACKNOWLEDGMENTS

This work was supported by the National Science Center (Grant 7873/B/P01/2011/40). M.R. was supported by the Foundation for Polish Science (Grant PARENT-BRIDGE/2011-3/2), cofinanced by the European Union Regional Development Fund. A.S. was supported by the National Science Center (Grant 2014/15/N/NZ4/01912). J.W. was supported by the National Science Center (Grant DEC-2012/06/M/NZ3/00163). G.W. was supported by the European Regional Development Fund (Grant POIG 01.01.02-00-008/08).

REFERENCES

Aoki K, Matsuda M (2009). Visualization of small GTPase activity with fluorescence resonance energy transfer-based biosensors. Nat Protoc 4, 1623–1631.

Barbour B, Keller BU, Llano I, Marty A (1994). Prolonged presence of glutamate during excitatory synaptic transmission to cerebellar Purkinje cells. Neuron 12, 1331–1343.

Beique JC, Lin DT, Kang MG, Aizawa H, Takamiya K, Huganir RL (2006). Synapse-specific regulation of AMPA receptor function by PSD-95. Proc Natl Acad Sci USA 103, 19535–19540.

Bilousova TV, Rusakov DA, Ethell DW, Ethell IM (2006). Matrix metalloproteinase-7 disrupts dendritic spines in hippocampal neurons through NMDA receptor activation. J Neurochem 97, 44–56.

Bourguignon LY (2008). Hyaluronan-mediated CD44 activation of RhoGTPase signaling and cytoskeleton function promotes tumor progression. Semin Cancer Biol 18, 251–259.

Bourguignon LY, Gilad E, Rothman K, Peyrollier K (2005). Hyaluronan-CD44 interaction with IQGAP1 promotes Cdc42 and ERK signaling, leading to actin binding, Elk-1/estrogen receptor transcriptional activation, and ovarian cancer progression. J Biol Chem 280, 11961–11972.

Bourguignon LY, Singleton PA, Zhu H, Diedrich F (2003). Hyaluronan-mediated CD44 interaction with RhoGEF and Rho kinase promotes Grb2-associated binder-1 phosphorylation and phosphatidylinositol 3-kinase signaling leading to cytokine (macrophage-colony stimulating factor) production and breast tumor progression. J Biol Chem 278, 29420–29434.

Bourguignon LY, Zhu H, Shao L, Chen YW (2000). CD44 interaction with tiam1 promotes Rac1 signaling and hyaluronic acid-mediated breast tumor cell migration. J Biol Chem 275, 1829–1838.

Bourguignon LY, Zhu H, Zhou B, Diedrich F, Singleton PA, Hung MC (2001). Hyaluronan promotes CD44v3-Vav2 interaction with Grb2-p185(HER2) and induces Rac1 and Ras signaling during ovarian tumor cell migration and growth. J Biol Chem 276, 48679–48692.

Bourne J, Harris KM (2007). Do thin spines learn to be mushroom spines that remember? Curr Opin Neurobiol 17, 381–386.

Bourne JN, Harris KM (2008). Balancing structure and function at hippocampal dendritic spines. Annu Rev Neurosci 31, 47–67.

Brummelkamp TR, Bernards R, Agami R (2002). A system for stable expression of short interfering RNAs in mammalian cells. Science 296, 550–553.

Cathala L, Holderith NB, Nusser Z, DiGregorio DA, Cull-Candy SG (2005). Changes in synaptic structure underlie the developmental speeding of AMPA receptor-mediated EPSCs. Nat Neurosci 8, 1310–1318.
Chen LY, Rex CS, Casale MS, Gall CM, Lynch G (2007). Changes in synaptic morphology accompany actin signaling during LTP. J Neurosci 27, 5363–5372.
Chetty C, Vanamala SK, Gondi CS, Dinh DH, Gujrati M, Rao JS (2012). MMP-9 induces CD44 cleavage and CD44 mediated cell migration in glioblastoma xenograft cells. Cell Signal 24, 549–559.
Conant K, Allen M, Lim ST (2015). Activity dependent CAM cleavage and neurotransmission. Front Cell Neurosci 9, 305.
Dalva MB, McClelland AC, Kayser MS (2007). Cell adhesion molecules: signalling functions at the synapse. Nat Rev Neurosci 8, 206–220.
Dansie LE, Ethell IM (2011). Casting a net on dendritic spines: the extracellular matrix and its receptors. Dev Neurobiol 71, 956–981.
Dityatev A, Rusakov DA (2011). Molecular signals of plasticity at the tetrapartite synapse. Curr Opin Neurobiol 21, 353–359.
Dityatev A, Schachner M (2003). Extracellular matrix molecules and synaptic plasticity. Nat Rev Neurosci 4, 456–468.
Ehrlich I, Klein M, Rumpel S, Malinow R (2007). PSD-95 is required for activity-driven synapse stabilization. Proc Natl Acad Sci USA 104, 4176–4181.
Ethell IM, Pasquale EB (2005). Molecular mechanisms of dendritic spine development and remodeling. Prog Neurobiol 75, 161–205.
Fogarty MJ, Hammond LA, Kanjhan R, Bellingham MC, Noakes PG (2013). A method for the three-dimensional reconstruction of Neurobiotin-filled neurons and the location of their synaptic inputs. Front Neural Circuits 7, 153.
Frischknecht R, Heine M, Perrais D, Seidenbecher CI, Choquet D, Gundelfinger ED (2009). Brain extracellular matrix affects AMPA receptor lateral mobility and short-term synaptic plasticity. Nat Neurosci 12, 897–904.
Groc L, Choquet D, Stephenson FA, Verrier D, Manzoni OJ, Chavis P (2007). NMDA receptor surface trafficking and synaptic subunit composition are developmentally regulated by the extracellular matrix protein. Reelin J Neurosci 27, 10165–10175.
Hall A, Nobes CD (2000). Rho GTPases: molecular switches that control the organization and dynamics of the actin cytoskeleton. Philos Trans R Soc Lond B Biol Sci 355, 965–970.
Hotulainen P, Hoogenraad CC (2010). Actin in dendritic spines: connecting dynamics to function. J Cell Biol 189, 619–629.
Hotulainen P, Llano O, Smirnov S, Tanhuanpaa K, Faix J, Rivera C, Lappalainen P (2009). Defining mechanisms of actin polymerization and depolymerization during dendritic spine morphogenesis. J Cell Biol 185, 323–339.
Itoh RE, Kurokawa K, Ohba Y, Yoshizaki H, Mochizuki N, Matsuda M (2002). Activation of rac and cdc42 video imaged by fluorescent resonance energy transfer-based single-molecule probes in the membrane of living cells. Mol Cell Biol 22, 6582–6591.
Jausoro I, Mestres I, Quassollo G, Masseroni L, Heredia F, Caceres A (2013). Regulation of spine density and morphology by IQGAP1 protein domains. PLoS One 8, e56574.
Jaworski J, Spangler S, Seeburg DP, Hoogenraad CC, Sheng M (2005). Control of dendritic arborization by the phosphoinositide-3′-kinase-Akt-mammalian target of rapamycin pathway. J Neurosci 25, 11300–11312.
Kasai H, Matsuzaki M, Noguchi J, Yasumatsu N, Nakahara H (2003). Structure-stability-function relationships of dendritic spines. Trends Neurosci 26, 360–368.
Kochlamazashvili G, Henneberger C, Bukalo O, Dvoretskova E, Senkov O, Lievens PM, Westenbroek R, Engel AK, Catterall WA, Rusakov DA, *et al.* (2010). The extracellular matrix molecule hyaluronic acid regulates hippocampal synaptic plasticity by modulating postsynaptic L-type Ca(2+) channels. Neuron 67, 116–128.
Koleske AJ (2013). Molecular mechanisms of dendrite stability. Nat Rev Neurosci 14, 536–550.
Konopacki FA, Rylski M, Wilczek E, Amborska R, Detka D, Kaczmarek L, Wilczynski GM (2007). Synaptic localization of seizure-induced matrix metalloproteinase-9 mRNA. Neuroscience 150, 31–39.
Konopka A, Zeug A, Skupien A, Kaza B, Mueller F, Chwedorowicz A, Ponimaskin E, Wilczynski GM, Dzwonek J (2016). Cleavage of hyaluronan and CD44 adhesion molecule regulate astrocyte morphology via Rac1 signalling. PLoS One 11, e0155053.
Kopec CD, Li B, Wei W, Boehm J, Malinow R (2006). Glutamate receptor exocytosis and spine enlargement during chemically induced long-term potentiation. J Neurosci 26, 2000–2009.
Lanore F, Blanchet C, Fejtova A, Pinheiro P, Richter K, Balschun D, Gundelfinger E, Mulle C (2010). Impaired development of hippocampal mossy fibre synapses in mouse mutants for the presynaptic scaffold protein Bassoon. J Physiol 588, 2133–2145.
Levy AD, Omar MH, Koleske AJ (2014). Extracellular matrix control of dendritic spine and synapse structure and plasticity in adulthood. Front Neuroanat 8, 116.
Lonskaya I, Partridge J, Lalchandani RR, Chung A, Lee T, Vicini S, Hoe HS, Lim ST, Conant K (2013). Soluble ICAM-5, a product of activity dependent proteolysis, increases mEPSC frequency and dendritic expression of GluA1. PLoS One 8, e69136.
Matsuzaki M, Honkura N, Ellis-Davies GC, Kasai H (2004). Structural basis of long-term potentiation in single dendritic spines. Nature 429, 761–766.
Mayhew TM, Lucocq JM (2008). Developments in cell biology for quantitative immunoelectron microscopy based on thin sections: a review. Histochem Cell Biol 130, 299–313.
Meng Y, Zhang Y, Tregoubov V, Janus C, Cruz L, Jackson M, Lu WY, MacDonald JF, Wang JY, Falls DL, Jia Z (2002). Abnormal spine morphology and enhanced LTP in LIMK-1 knockout mice. Neuron 35, 121–133.
Michaluk P, Wawrzyniak M, Alot P, Szczot M, Wyrembek P, Mercik K, Medvedev N, Wilczek E, De Roo M, Zuschratter W, *et al.* (2011). Influence of matrix metalloproteinase MMP-9 on dendritic spine morphology. J Cell Sci 124, 3369–3380.
Missler M, Sudhof TC, Biederer T (2012). Synaptic cell adhesion. Cold Spring Harb Perspect Biol 4, a005694.
Murakoshi H, Wang H, Yasuda R (2011). Local, persistent activation of Rho GTPases during plasticity of single dendritic spines. Nature 472, 100–104.
Murakoshi H, Yasuda R (2012). Postsynaptic signaling during plasticity of dendritic spines. Trends Neurosci 35, 135–143.
Nakayama AY, Harms MB, Luo L (2000). Small GTPases Rac and Rho in the maintenance of dendritic spines and branches in hippocampal pyramidal neurons. J Neurosci 20, 5329–5338.
Ning L, Tian L, Smirnov S, Vihinen H, Llano O, Vick K, Davis RL, Rivera C, Gahmberg CG (2013). Interactions between ICAM-5 and beta1 integrins regulate neuronal synapse formation. J Cell Sci 126, 77–89.
Noguchi J, Nagaoka A, Watanabe S, Ellis-Davies GC, Kitamura K, Kano M, Matsuzaki M, Kasai H (2011). In vivo two-photon uncaging of glutamate revealing the structure-function relationships of dendritic spines in the neocortex of adult mice. J Physiol 589, 2447–2457.
Otmakhov N, Khibnik L, Otmakhova N, Carpenter S, Riahi S, Asrican B, Lisman J (2004). Forskolin-induced LTP in the CA1 hippocampal region is NMDA receptor dependent. J Neurophysiol 91, 1955–1962.
Peixoto RT, Kunz PA, Kwon H, Mabb AM, Sabatini BL, Philpot BD, Ehlers MD (2012). Transsynaptic signaling by activity-dependent cleavage of neuroligin-1. Neuron 76, 396–409.
Ponta H, Sherman L, Herrlich PA (2003). CD44: from adhesion molecules to signalling regulators. Nat Rev Mol Cell Biol 4, 33–45.
Raber J, Olsen RH, Su W, Foster S, Xing R, Acevedo SF, Sherman LS (2014). CD44 is required for spatial memory retention and sensorimotor functions. Behav Brain Res 275, 146–149.
Rex CS, Chen LY, Sharma A, Liu J, Babayan AH, Gall CM, Lynch G (2009). Different Rho GTPase-dependent signaling pathways initiate sequential steps in the consolidation of long-term potentiation. J Cell Biol 186, 85–97.
Sala C, Segal M (2014). Dendritic spines: the locus of structural and functional plasticity. Physiol Rev 94, 141–188.
Saneyoshi T, Fortin DA, Soderling TR (2010). Regulation of spine and synapse formation by activity-dependent intracellular signaling pathways. Curr Opin Neurobiol 20, 108–115.
Shi Y, Ethell IM (2006). Integrins control dendritic spine plasticity in hippocampal neurons through NMDA receptor and Ca2+/calmodulin-dependent protein kinase II-mediated actin reorganization. J Neurosci 26, 1813–1822.
Skupien A, Konopka A, Trzaskoma P, Labus J, Gorlewicz A, Swiech L, Babraj M, Dolezyczek H, Figiel I, Ponimaskin E, *et al.* (2014). CD44 regulates dendrite morphogenesis through Src tyrosine kinase-dependent positioning of the Golgi. J Cell Sci 127, 5038–5051.
Song I, Semyanov A (2011). Single cell electrophysiologic recordings in hippocampal slices. Protocol Exchange 2011, doi:10.1038/protex.2011.253.
Szepesi Z, Bijata M, Ruszczycki B, Kaczmarek L, Wlodarczyk J (2013). Matrix metalloproteinases regulate the formation of dendritic spine head protrusions during chemically induced long-term potentiation. PLoS One 8, e63314.
Szepesi Z, Hosy E, Ruszczycki B, Bijata M, Pyskaty M, Bikbaev A, Heine M, Choquet D, Kaczmarek L, Wlodarczyk J (2014). Synaptically released

matrix metalloproteinase activity in control of structural plasticity and the cell surface distribution of GluA1-AMPA receptors. PLoS One 9, e98274.
Tada T, Sheng M (2006). Molecular mechanisms of dendritic spine morphogenesis. Curr Opin Neurobiol 16, 95–101.
Taft CE, Turrigiano GG (2014). PSD-95 promotes the stabilization of young synaptic contacts. Philos Trans R Soc Lond B Biol Sci 369, 20130134.
Tashiro A, Minden A, Yuste R (2000). Regulation of dendritic spine morphology by the rho family of small GTPases: antagonistic roles of Rac and Rho. Cereb Cortex 10, 927–938.
Tashiro A, Yuste R (2004). Regulation of dendritic spine motility and stability by Rac1 and Rho kinase: evidence for two forms of spine motility. Mol Cell Neurosci 26, 429–440.
Thalhammer A, Cingolani LA (2014). Cell adhesion and homeostatic synaptic plasticity. Neuropharmacology 78, 23–30.
Tonnesen J, Katona G, Rozsa B, Nagerl UV (2014). Spine neck plasticity regulates compartmentalization of synapses. Nat Neurosci 17, 678–685.
Vadodaria KC, Brakebusch C, Suter U, Jessberger S (2013). Stage-specific functions of the small Rho GTPases Cdc42 and Rac1 for adult hippocampal neurogenesis. J Neurosci 33, 1179–1189.
Wang XB, Bozdagi O, Nikitczuk JS, Zhai ZW, Zhou Q, Huntley GW (2008). Extracellular proteolysis by matrix metalloproteinase-9 drives dendritic spine enlargement and long-term potentiation coordinately. Proc Natl Acad Sci USA 105, 19520–19525.
Wilczynski GM,, Wilczek E, Lasiecka Z, Gorlewicz A, Michaluk P, Wawrzyniak M, Malinowska M, Okulski P, Kolodziej LR (2008). Important role of matrix metalloproteinase 9 (MMP-9) in epileptogenesis. J Cell Biol 180, 1021–1035.
Wlodarczyk J, Mukhina I, Kaczmarek L, Dityatev A (2011). Extracellular matrix molecules, their receptors, and secreted proteases in synaptic plasticity. Dev Neurobiol 71, 1040–1053.
Yang Y, Wang XB, Frerking M, Zhou Q (2008). Spine expansion and stabilization associated with long-term potentiation. J Neurosci 28, 5740–5751.
Yoshizaki H, Ohba Y, Kurokawa K, Itoh RE, Nakamura T, Mochizuki N, Nagashima K, Matsuda M (2003). Activity of Rho-family GTPases during cell division as visualized with FRET-based probes. J Cell Biol 162, 223–232.
Yuste R, Bonhoeffer T (2001). Morphological changes in dendritic spines associated with long-term synaptic plasticity. Annu Rev Neurosci 24, 1071–1089.